ACS Photonics

Article

pubs.acs.org/journal/apchd5

Versatile Optical Fiber Nanoprobes: From Plasmonic Biosensors to Polarization-Sensitive Devices

Armando Ricciardi,[†,‡] Marco Consales,[†,‡] Giuseppe Quero,[‡] Alessio Crescitelli,[§] Emanuela Esposito,*[,§] and Andrea Cusano*[,‡]

[‡]Optoelectronic Division, Department of Engineering, University of Sannio, I-82100, Benevento, Italy

[§]Istituto per la Microelettronica e Microsistemi, National Council of Research, I-80131 Napoli, Italy

ABSTRACT: We have recently proposed a valuable fabrication route for the integration and patterning of functional materials at nanoscale onto optical fibers, posing the basis for a new technological vision named "Lab-on-Fiber". The validation of the proposed process has been carried out through the realization, directly onto the fiber tip, of 2D metallo-dielectric nanocrystals supporting localized surface plasmon resonances. In this work, we demonstrate the effectiveness of the proposed methodology to realize optical nanoprobes for label-free chemical and biological sensing as well as basic components for novel polarization sensitive photonic devices. Specifically, we first demonstrate how it is possible to tailor the field distribution of the plasmonic mode enabling the control on the refractive index sensitivity. With a view toward surface sensitivity, we experimentally observe that the proposed device is able to detect the formation of nanosized overlays over very limited active areas. Moreover, we demonstrate how to control the number and the field distribution of the excited plasmonic resonance posing new basis for the resonance engineering. Finally, we show how to obtain polarization sensitive devices with the same technological platform, by breaking the circular crystal symmetry at both unit cell or entire lattice level.

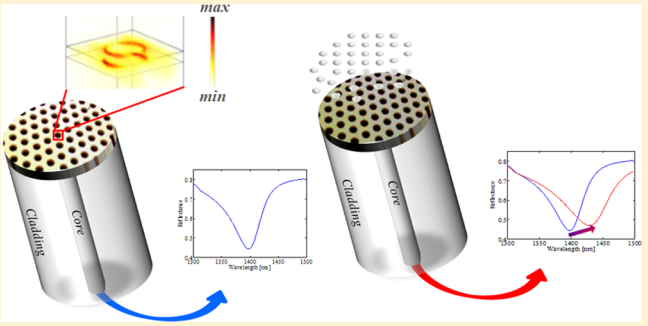

KEYWORDS: *lab-on-fiber, nanofabrication, localized surface plasmon resonances (LSPRs), chemical and biological sensing, polarization-sensitive devices*

INTRODUCTION

Optical fibers technology has experienced a tremendous growth and advancement over the past several decades, not only in transmission systems for communications (where nowadays totally dominate especially at the high performances level), but also in the sensing field.[1] For this reason, there is an ever increasing need to add new functionalities and improve the performances, through the integration on the optical fibers of advanced functional materials providing the control and manipulation of light at nanoscale. Both metallic and dielectric nanostructures (in particular, photonic and plasmonic crystals) seem to meet that need since they offer unprecedented opportunities for subwavelength field confinement[2] and resonant field enhancement.[3] These unique characteristics have been hitherto exploited in many applications (ranging from surface-enhanced Raman scattering[4−6] to nonlinear optics[7−10] and energy harvesting[11,12]) and have witnessed, for instance, the consolidation of the lab-on-chip technology. Many prestigious research groups in the photonic community are thus focusing their efforts to fuse together the world of nanotechnology with optical fibers, leading to the development of a novel and intriguing technology known as "Lab-on-Fiber".[13] The integration of nanostructures within optical fibers is giving rise to a new generation of highly functionalized all in-fiber nanoprobes which, being easily and remotely connectable to complex illumination systems and demodulation units, may partially overcome the issue related to the extreme integration of all the components required at the lab-on-chip level.[13−16]

In order to address the fabrication issues and adapt modern nanotechnologies facilities to properly work on unconventional substrates such as the case of optical fibers, different strategies, and processes have been recently proposed.[17−28] Among them, we have demonstrated a reliable fabrication path which allows to integrate on a standard single mode optical fiber tip both metal and dielectric materials patterned at micro and nanoscale by means of a direct writing approach.[27] To demonstrate the strength of our method, we fabricated and characterized a first lab-on-fiber platform (schematically represented in Figure 1a) based on a 2D hybrid metallo-dielectric nanostructure supporting localized surface plasmon resonances (LSPRs).[27]

In this work, we demonstrate the versatility and potentialities of the proposed platform to work as both label-free chemical and biological sensor as well as polarization-dependent wavelength-selective photonic nanodevice.

The paper is mainly divided into two parts. The first part deals with the analysis of the sensitivity to the surrounding refractive index (SRI) changes; in particular, we experimentally

Received: October 11, 2013
Published: November 29, 2013

 © 2013 American Chemical Society dx.doi.org/10.1021/ph400075r | *ACS Photonics* 2014, 1, 69−78

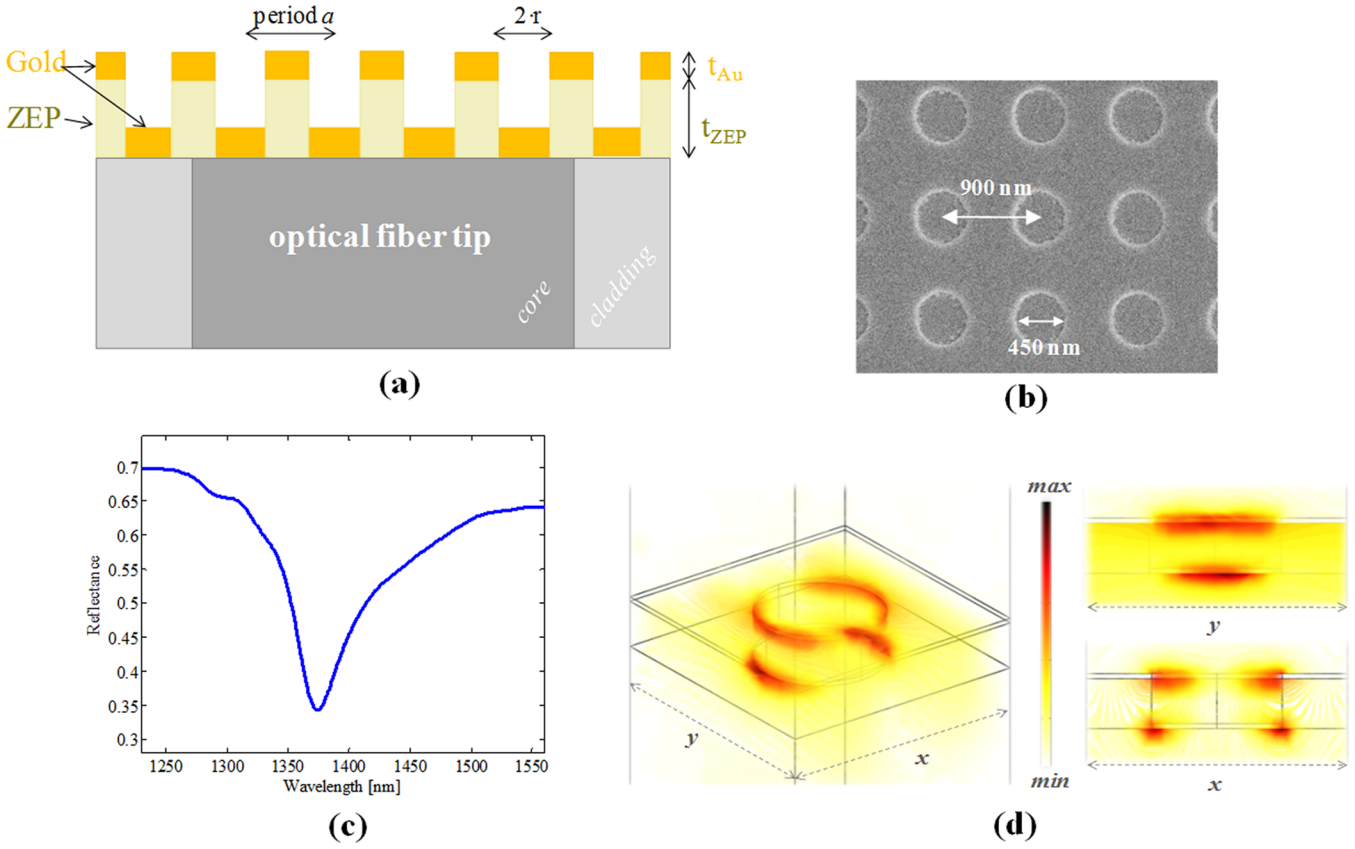

Figure 1. (a) Cross section schematic view of the hybrid metallo-dielectric nanostructure and (b) SEM top view image of the realized device; (c) Measured reflectance spectrum of the hybrid fiber tip device characterized by period a = 900 nm, t_{ZEP} = 200 nm, and t_{Au} = 20 nm; (d) near field map in correspondence of the resonant wavelength, numerically evaluated in the unit cell domain.

study the dependence of the *bulk* SRI sensitivity on both physical and geometrical parameters, including the lattice tiling (we analyze both periodic and aperiodic patterns). Moreover, by having in mind practical scenarios of label-free biological sensing, we evaluate the *surface* sensitivity (i.e., when nanosized overlays are deposited on the top of the device) and prove that the sensitive area can be reduced down to 20 × 20 μm^2 around the fiber core without affecting the device performances.

The second part of the paper is devoted to the plasmonic resonance engineering. We show how it is possible to control both the number and the near field distribution of the excited LSPRs opening new options for sensitivity tuning. Finally, we experimentally explore the possibility of creating novel polarization sensitive wavelength-selective optical fiber devices, by breaking the circular symmetry of the crystal nanostructure at both unit cell or entire lattice levels (in particular by introducing elliptical holes or a period mismatch in the two perpendicular directions). As discussed below, these two approaches produce different effects on the spectral features of the device useful for creating polarization mirror, filters and modulators completely integrated into optical fibers.

RESULTS AND DISCUSSION

Bulk Refractive Index Sensitivity. With reference to Figure 1, we start our analysis by considering a structure made of a ZEP 520A (methyl styrene/chloromethyl acrylate copolymer) layer (having a thickness t_{ZEP} = 200 nm) patterned with a square lattice (with period a = 900 nm) of circular holes (with radius r = 225 nm) and covered with a gold film (with thickness t_{Au} = 20 nm) deposited on both the ridges and the grooves. The top view SEM image of the fabricated device is shown in Figure 1b). Details on the fabrication procedure can be found in Methods. By illuminating our probe in out-of-plane configuration (as the case of single mode fiber in the paraxial propagation regime), the experimental reflectance spectrum (shown in Figure 1c) exhibits a resonance dip (centered at 1374 nm with a *Q*-factor of about 23) due to the excitation of a LSPR. In fact, Figure 1d shows the near field map in correspondence of the resonant wavelength, numerically evaluated in the unit cell domain by means of the commercial software COMSOL Multiphysics.[29] Details on the numerical simulation can be also found in Methods. It is evident that the field is highly localized both around the gold pillar (on the bottom) and the gold slab holes (on the top), meaning that is present a sort of interaction between two plasmonic modes.

The excitation wavelengths of LSPRs are very sensitive to environment modifications,[30] thus, any change in the SRI around the fiber tip, causes a wavelength shift of the resonant dip, making the device particularly suited for label-free chemical sensing and biosensing.

From Figure 1a it can be easily noticed how the gold layer deposited on the top of the fiber tip device shields the plasmonic mode excited within the hybrid crystal from the external environment, thus, limiting the device sensitivity. It is therefore reasonable to expect that a reduction of the gold overlay thickness would promote an enhancement of the light-matter interaction with the surroundings and improve the SRI sensing performances.

dx.doi.org/10.1021/ph400075r | ACS Photonics 2014, 1, 69−78

To experimentally verify this assumption, we tested three fiber optic probes with different gold layer thickness, t_{Au} = 20, 30, and 40 nm, keeping constant the other geometrical parameters (a = 900 nm, r = 225 nm, and t_{ZEP} = 200 nm). In order to avoid small discrepancies in the hole radii and in the ZEP layer thickness that may occur from sample to sample due to fabrication tolerances, the same fiber tip probe was used, initially coated by a 20 nm thick gold layer, on which two further gold depositions of ∼10 nm each have been successively carried out.

Successively we analyzed the SRI sensitivity by immersing the probes in liquid solutions with different RI, that is, water (n = 1.333), ethanol (n = 1.362), and isopropyl alcohol (n = 1.378), and measured the resonant wavelength shift ($\Delta\lambda_{min}$) occurring upon immersion. We have investigated this RI range (around that of water) in view of the potential applicability of our probe to biological applications that will be better discussed below. Indeed, the considered range widely includes the RI of most biological (buffered) environments, for example, phosphate buffer solutions at pH = 5 (RI ∼ 1.344 at λ = 589 nm) or pH = 7 (RI ∼ 1.348 at λ = 589 nm), typically used in real scenarios.

In Figure 2a the characteristic curves ($\Delta\lambda_{min}$ vs SRI) of the three samples having t_{Au} = 20, 30, and 40 nm, respectively, have been reported. Obtained results are in line with our numerical predictions,[27] confirming that SRI sensitivity increases as a consequence of a reduction of t_{Au}. Indeed, as reported in Figure 2a, it increases from 36 nm/RIU to 98 nm/RIU by passing from a gold layer thickness of 40 to 30 nm and from 98 nm/RIU to 125 nm/RIU by passing from t_{Au} = 30 nm to t_{Au} = 20 nm. In the linear fitting approximation (red line in Figure 2b), a sensitivity increase of ∼4.5 nm/RIU per nanometer of gold layer has been estimated. As a consequence, an additional improvement could be hypothetically obtained up to ∼170 nm/RIU with t_{Au} = 10 nm. However, the reduction of the gold layer thickness has already been demonstrated to produce a red-shift of the resonant dip, combined to its bandwidth widening and visibility reduction.[27] Although with a gold layer thickness of 20 nm, the reflectance dip in the spectrum is still present and visible, a further reduction of the gold thickness would produce an additional decrease in the resonance visibility, thus, compromising the capability of detecting the resonant wavelength shift occurring upon SRI changes.

Nevertheless, at a first comparison with respect to the state of the art of LSPR-based fiber tip devices, our sensitivity results are almost comparable to that demonstrated in ref 25 by fiber optic sensor based on ordered array of gold nanodots (195 nm/RIU) and 4-fold lower to that exhibited in ref 24 by a fiber tip-sensor based on arrays of gold sub wavelengths apertures (500 nm/RIU). In our case, however, the resonance shows a much higher Q factor (of about 90%) and has a significantly smaller active area since we use single- instead of multimode optical fibers. In light of these considerations, it is important to remark, as it will be better discussed later, that when dealing with sensing devices for label free biosensing, also the active area (in addition to the sensitivity and the Q-factor for the resolution) plays a fundamental role since for a given local RI change, a larger amount of bound biomolecules is required for larger active area platforms. Finally, thanks to the versatility of our technological platform, we can act on the large set of available parameters (e.g., ZEP layer thickness, suitable dielectric patterns, size of the active area, etc.) to further improve the final device characteristics.

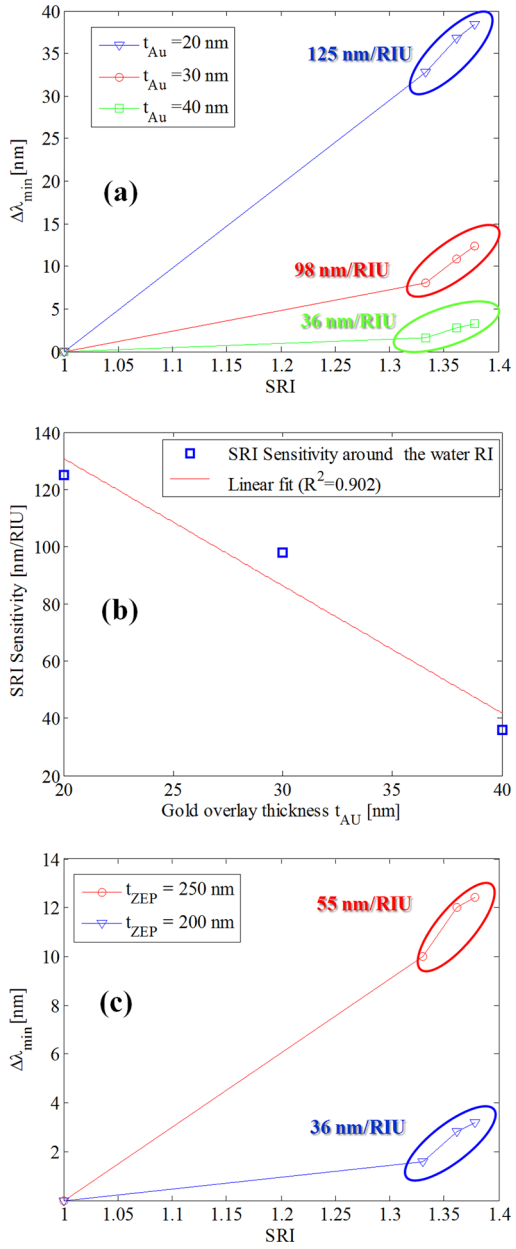

Figure 2. (a) $\Delta\lambda_{min}$ as a function of the SRI for three fiber optic probes characterized by t_{Au} = 20 nm (blue triangles), t_{Au} = 30 nm (red circles), and t_{Au} = 40 nm (green squares); (b) Variation of the SRI sensitivity as a function of t_{Au}, around the water RI; (c) $\Delta\lambda_{min}$ as a function of the SRI for two fiber optic probes characterized by t_{Au} = 40 nm, a = 900 nm, r/a = 0.25, and having two different values of the ZEP overlay thickness, 200 nm (blue triangles) and 250 nm (red circles).

For example, as shown in Figure 2c, a bulk SRI sensitivity of 55 nm/RIU was found for a structure having a slightly thicker ZEP overlay (t_{ZEP} = 250 nm) with the same period (a = 900 nm), filling factor (r/a = 0.25), and gold thickness (t_{Au} = 40 nm). Hence, an improvement of ∼40% has been obtained with an increase of ∼50 nm in the ZEP layer thickness.

Sensitivity Enhancement with Quasicrystals. On the basis of some recent results demonstrating the capability of hybrid metallo-dielectric quasicrystals (QCs) to outperform their periodic counterparts in chemical sensing applications,[31,32] we also investigated the use of quasiperiodic tiling as a mean to improve the SRI sensitivity of the proposed device. In

dx.doi.org/10.1021/ph400075r | ACS Photonics 2014, 1, 69−78

particular, here we show some preliminary results of a metallo-dielectric QC directly realized on the fiber tip according to the Ammann-Beenker (octagonal) tiling.[33]

The top view SEM image of the fabricated structure (characterized by an equivalent period a = 900 nm, t_{ZEP} = 250 nm, and t_{Au} = 40 nm) is shown in Figure 3a. In Figure 3b

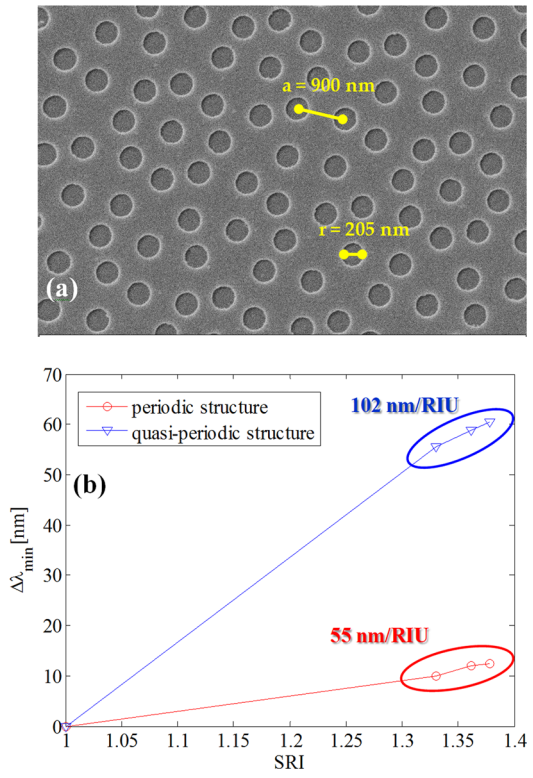

Figure 3. (a) SEM image of the hybrid metallo-dielectric QC structure directly realized on the fiber tip; (b) $\Delta\lambda_{min}$ as a function of the SRI obtained with a quasi-periodic and periodic structure having same filling factor (r/a = 0.25), a = 900 nm, t_{ZEP} = 250 nm, and t_{Au} = 40 nm.

we have reported the relative wavelength shifts of the LSPR dip of such a structure as a function of the SRI. For comparison, the wavelength shift obtained with a periodic sample (its periodic counterpart) characterized by the same lattice period, ZEP, and gold overlay thickness, as well as the same filling factor have also been shown. It turned out that for a given filling factor, QC-based devices are able to outperform (SRI sensitivities of 102 nm/RIU) their periodic counterpart (SRI sensitivities of 55 nm/RIU), with a sensitivity improvement of about a factor of 2.

Reported results, although still preliminary, lay the foundations for the development of a fiber optic nanoprobes based on aperiodic geometries, opening up different perspectives to obtain a full resonance engineering and control.[34] As a matter of fact, by using aperiodically ordered QC lattices, it could be possible to achieve richer resonant phenomena (with respect to the periodic case), enabling the selection of number and spectral localization of plasmonic resonances, which in turn can be designed to exhibit high quality factors, high sensitivities, and tuning efficiencies.[34] Moreover QCs may provide a better control on resonant coupling/uncoupling mechanisms by selectively breaking the lattice mirror symmetries via a judicious introduction of point defects.[35]

Surface RI Sensitivity. In practical scenarios related to label-free chemical and biological sensing applications, the top metal surface is functionalized with bioreceptors, chosen for their specific affinity toward a given biomolecule to provide the biorecognition feature. As a consequence, because of the binding of an analyte molecules layer, the RI changes are restricted to local modifications occurring at the sensor surface. Sensors based on LSPR, thanks to the highly localized character of its field distribution at the resonant wavelength, are well suited for detecting these local environment changes.

Accordingly, in this section, we experimentally evaluate the *surface* sensitivity of our optical fiber nanoprobe by depositing on its surface nanosized overlays mimicking local RI changes.

To this aim, by using the RF sputtering deposition technique we deposited on the top of the structure a ∼100 nm thick layer of SiO_2, whose refractive index ($n \sim 1.45$) well resembles that of most biological molecules.[36,37] The sample, in this case, is characterized by t_{ZEP} = 70 nm and t_{Au} = 20 nm. The reflectance spectra of a SiO_2-coated and uncoated fiber tip device are shown in Figure 4, where the experimental data have been also

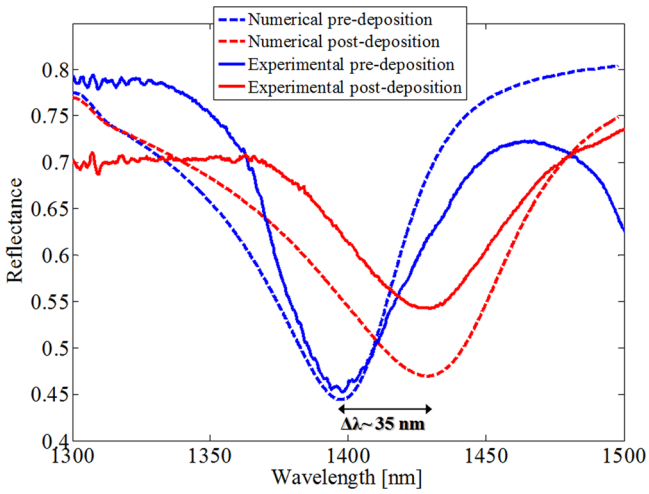

Figure 4. Numerical and experimental spectra of a hybrid nanostructure with t_{ZEP} = 70 nm and t_{Au} = 20 nm, before and after the SiO_2 coating deposition.

compared with those obtained by a numerical analysis.[27] A significant red-shift ($\Delta\lambda \sim 35$ nm) of the resonant wavelength occurs as a consequence of the surface layer deposition on both the ridges and the grooves of the structure.

This result reveals the promising capability of the proposed platform for detecting molecular monolayers at nanoscale; the resonance shift per nanometer of deposited overlay turns out (assuming a linear relationship between the wavelength shift and the overlay thickness) as high as 0.35 nm per nm of deposited SiO_2. This surface sensitivity is comparable to that achieved with nanostructured metallo-dielectric crystals realized on planar substrates, for which values up to ∼0.4 nm per nm of deposited SiO_2 have been found.[31] Results here provided once more demonstrate the great potentialities of the proposed Lab-on-Fiber platform, which allows to move devices from planar substrates to fiber tip (with all the related advantages) without affecting their performances. Considering the typical sizes of biological molecules (3.8−5.2 nm), it can be inferred that the binding of a single biological monolayer to the sample surface is able to generate a LSPR shift of approximately 1.3−1.8 nm, which may be easily detected via low-cost commercial

dx.doi.org/10.1021/ph400075r | ACS Photonics 2014, 1, 69−78

spectrophotometer. Although a concrete demonstration of the capability of our probe to work as a biosensor would require the demonstration of its ability to detect the formation of an ultrathin biomolecular layer upon its functionalized surface (via a detectable resonant wavelength shift), nevertheless, the achieved surface sensitivity is the first important step proving the potentialities of our platform for biosensing applications.

Sensing Area. As previously mentioned, it is important to remark that, when dealing with sensing platforms for label free biosensing, the active sensing area is a very important parameter that determines the performances of the final device. Indeed, if the biodetection experiment features an excess (very high concentration) of target biomolecules, then the sensing area size (regardless its extent) is not a key-point since the active region can be completely covered through the correct biofunctionalization of the probe surface. However, in many important practical cases (drug resistance recognition, early detection of cancer pathologies, and pathogen agents, as well as infections), there is the need for detecting a very small concentration of target biomolecules. For these applications, a given local refractive index change (on the sensor surface) is provided by a smaller amount of bound biomolecules if biosensors with reduced sensing areas are used. In other words, reducing the active area leads to a lowering of the limit of detection (LOD) in terms of absolute bound molecular mass.[38]

Moreover, one might wonder how many periods (or how many holes) of the photonic/plasmonic structure are necessary to achieve a strong coupling effect or equivalently a well-defined spectral feature in the reflectance spectrum.

Based on the above considerations, in the following we discuss the effects induced by the confinement of the ZEP overlay on the spectral resonant feature. To this aim, we used a UV-laser micromachining to gradually reduce (in successive steps) the patterned area of the device (characterized by a = 850 nm, t_{ZEP} = 200 nm, and t_{Au} = 40 nm) to 50 × 50 μm^2, 20 × 20 μm^2, and 10 × 10 μm^2 square region. The reflectance spectra relative to each confinement step are shown in Figure 5.

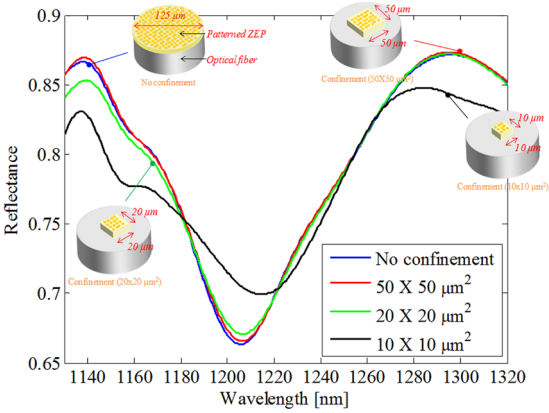

Figure 5. Reflectance spectra of the hybrid nanostructure, having a = 850 nm, t_{ZEP} = 200 nm, and t_{Au} = 40 nm, before and after the patterned area confinement (via UV-laser micromachining).

We can observe how, in the case of 50 × 50 μm^2 and 20 × 20 μm^2 confinements, the reflectance spectra (red and green curves) do not undergo any substantial modification with respect to the original one (blue curve); in other words, the patterned area reduction does not modify the field distribution of the excited LSPR, which remains confined in the horizontal plane in that area. On the contrary, when the patterned surface over the fiber core (diameter ∼ 8 μm) is reduced down to 10 × 10 μm^2, it is possible to observe a more pronounced variation of the corresponding reflectance spectra (black curve). From the above analysis it can be deduced that patterned area on the optical fiber tip can be reduced down to 20 × 20 μm^2 without any significant variations in the reflectance spectrum and consequently on the SRI sensitivity.

With respect to other LSPR-based fiber tip-devices, our sensing area is almost comparable (as also the bulk SRI sensitivity is) to that of the fiber optic sensor based on ordered array of gold nanodots[25] which uses single-mode optical fibers, whereas it is much smaller (400 μm^2 vs at least 2500 μm^2) than that exhibited by the fiber tip-sensor based on arrays of gold sub wavelengths apertures.[24] In this case, even though our device is characterized by a four time lower SRI sensitivity, however, it has a significantly smaller sensing area that allows to improve the biomolecules mass LOD. It is useful to point out that, in typical label-free biological applications, the sensor surface is chemically functionalized to support the binding of the target analyte on the biological recognition element only and specifically onto the active sensing area. In our device, this functionalization involves only the photonic/plasmonic area excluding the host material around it (i.e., the optical fiber).

Resonance Engineering. The analysis carried out so far is based on a single resonant dip occurring in the reflection spectra and associated to the excitation of a single LSPR. If small perturbations of the geometrical parameters in the metallo dielectric structure are introduced, then a slight change of the phase matching condition (i.e., the resonant wavelength and the coupling coefficient) for the single LSPR occurs. Nevertheless, if larger perturbations are taken into account, multiple LSPRs can be excited at different wavelengths, each one characterized by a specific field distribution and thus by a specific light matter interaction level, leading to the possibility of tailoring and eventually improving the device performances for the specific application.

Influence of the Slab Thickness. Here, just as an example, a resonance engineering approach able to influence both the number and the modal distribution of the resonances (excited in a given wavelength range) is demonstrated by considering ZEP overlay thicknesses higher than those previously considered. In Figure 6 we report the results of a numerical analysis aimed at investigating the evolution of the spectral response of our fiber tip device when the ZEP overlay thickness is varied between 300 and 600 nm (the other parameters are a = 900 nm, t_{Au} = 30 nm, r/a = 0.25). In particular, we show the contour plot of our device reflectance versus the ZEP layer thickness (Figure 6a) combined with the 3D views of unit cell and electric field distributions evaluated at the reflectance dip wavelengths for three different values of t_{ZEP}, that is, 300, 450, and 550 nm.

Reported results demonstrate that when ZEP layer thicknesses below ∼400 nm are considered, only one reflection dip appears within the reflectance spectrum, corresponding to only one resonance excited by the hybrid nanostructure, characterized by an electric field distribution localized both on the grating ridges and grooves (as previously shown in Figure 1d). However, when t_{ZEP} values higher than 400 nm are considered, richer spectra can be obtained, with two distinctive resonant dips appearing in the reflectance spectrum, corresponding to the excitation of two different LSPRs (see Figure 6b): the first one, at smaller wavelengths, exhibiting (as evident

dx.doi.org/10.1021/ph400075r | ACS Photonics 2014, 1, 69−78

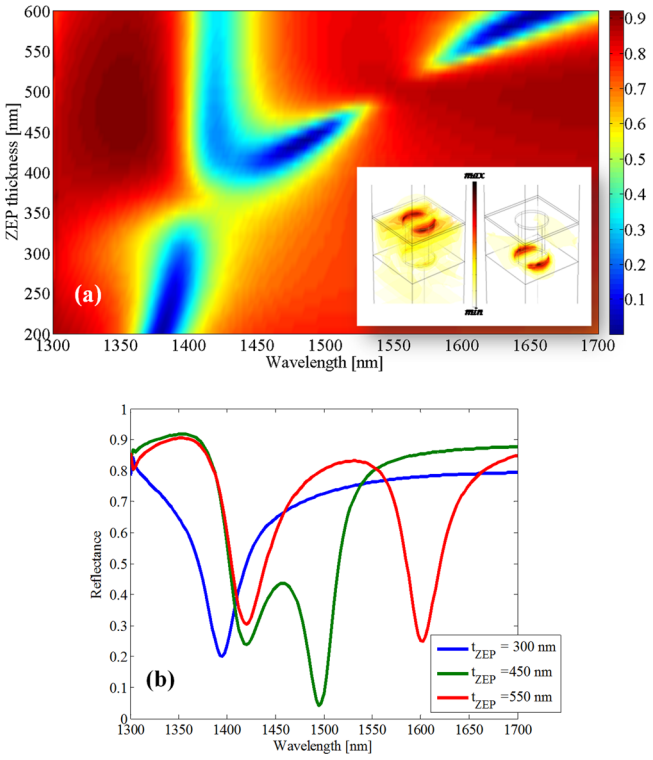

Figure 6. Contour plots of fiber tip reflectance versus the ZEP layer thickness; (inset) 3D view of unit cell and electric field distributions evaluated at the reflectance dip wavelengths for t_{ZEP} = 550 nm; (b) reflectance spectra extracted from the contour plot for t_{ZEP} = 300, 450, and 550 nm.

from its field distribution reported in the inset of Figure 6a) an electric field localized at the top plasmonic crystal (gold voids-like structure), which is independent from t_{ZEP} (the resonance is centered at λ = 1420 nm for t_{ZEP} = 450 and 550 nm, as shown in Figure 6b); the second one, at longer wavelengths, is characterized by a field distribution localized at the bottom (gold pillars-like) structure (see inset of Figure 6a); the resonant wavelength λ_{min} in this case moves toward higher wavelengths as the ZEP layer increases (specifically from 1495 to 1600 nm when t_{ZEP} changes from 450 to 550 nm).

Our results demonstrate that by choosing thicker enough dielectric overlays, we are able to split the single LSPR (i.e., the one reported in Figure 1c) into two resonances characterized by different electric field distributions and, consequently, different sensitivities to the SRI variations. This phenomenon could have a practical implication also for biological sensing; since immobilization/binding of surface bioreceptors/target molecules can occur in different forms to specific sites on the nanograting surface (i.e., over the grating ridges and grooves), the excitation of different resonant modes with distinctive near field distributions could be very useful also for gathering information on the geometrical arrangement of bioreceptors/target biomolecules layer. In fact, a significant wavelength shift is expected only for that resonances whose near field distribution strongly interact with the immobilized/bound biolayer.

Overall, the possibility to control the electric field distribution of the resonant mode with the ZEP thickness can be used for achieving different degrees of sensitivity to the external medium variation; The insensitive resonance could be used for example as reference channel or as a compensator in sensing applications.

Polarization Sensitive Devices. The results presented so far pertain to a polarization independent structure; as matter of fact, the spectral response of the device does not depend on the polarization state of the incoming light because of the rotational symmetry of the 2D lattice placed on the optical fiber tip. It is clear that polarization independent operation is desirable in most cases.

However, in polarization conversion and power equalization applications, devices providing the state of polarization control are of primary importance. For example, the polarization control is crucial for avoiding signal fading in fiber interferometric sensors or for creating polarization modulators.

Our technological platform lends itself well to the polarization management if the aforementioned crystal circular rotational symmetry is broken. This can be attained by following two different approaches (eventually combined together): the first one concerns the crystal structure at unit cell level through the definition of elliptical holes in such a way that the two perpendicular polarization states can interact with different crystal radii; the other possibility is to act at the entire lattice level creating a period asymmetry along the two perpendicular directions of the crystal. In the following, we discuss about the plasmonic resonance effect relative to these two configurations and show how they differently affect the spectral response of the final device.

Holes Ellipticity. We have fabricated and tested a first device (see the top-view SEM image in Figure 7a) consisting of a square lattice of *elliptical* holes with lattice period a = 900 nm and radii along the x and y axes, respectively, of r_x = 225 nm and r_y = 337.5 nm (ellipticity coefficient η = 1.5). The dielectric and metal thicknesses are t_{ZEP} = 100 nm and t_{Au} = 20 nm.

In Figure 7b,c we report the numerical and experimental reflectance spectra of the sample for different incident wave polarizations, demonstrating a good agreement. When the electric field is polarized along the x axis (POL_x) the reflectance spectrum shows one well-defined dip (red line) centered at around 1400 nm; vice versa, the spectrum referring to POL_y (blue line) exhibits high reflectivity in the whole analyzed wavelength range without any significant resonant effect. This behavior can be explained by the fact that the two different polarizations experience the same lattice period, but two different values of the holes radius (along the two symmetry axes); specifically, in the first case, the x-polarized incoming light interact with the "optimized" structure (r/a = 0.25) supporting the LSPR and guaranteeing the maximum resonance visibility. For the POL_y, since the radius is higher, an almost uniform gold layer is created on the optical fiber tip, thus, causing the incident light to be strongly reflected with very small interaction with the external structure. If the incident electric field polarization gradually moves from POL_x to POL_y, the resonant phenomenon becomes weaker with a consequent significant reduction of the resonance visibility, also accompanied by a slight blue wavelength shift. By changing the polarization input light, the reflected light intensity can be linearly tuned from ~20 to ~60%.

Overall, if hole ellipticity is introduced in the crystal lattice, our device works as a polarization sensitive in-fiber mirror that strongly reflects only one polarization component and absorbs the other.

Period Asymmetry. We have also characterized a second sample based on a lattice of circular holes spaced by two

dx.doi.org/10.1021/ph400075r | ACS Photonics 2014, 1, 69−78

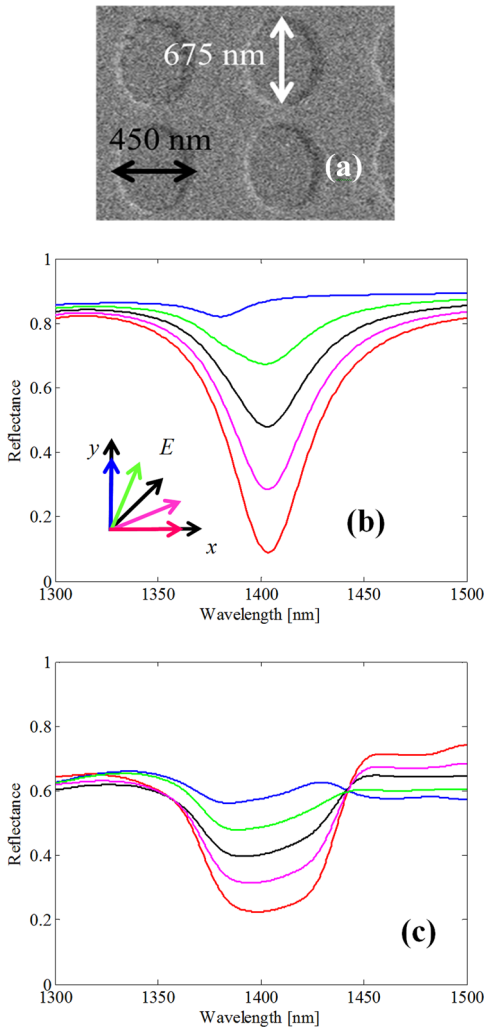

Figure 7. (a) SEM image (top view, zoomed) of the PCC probe with elliptical holes (r_x = 225 nm, r_y = 337.5 nm); (b) numerical and (c) experimental reflectance spectra of sample A for different incident wave polarizations: blue and red lines refer to POL_x and POL_y.

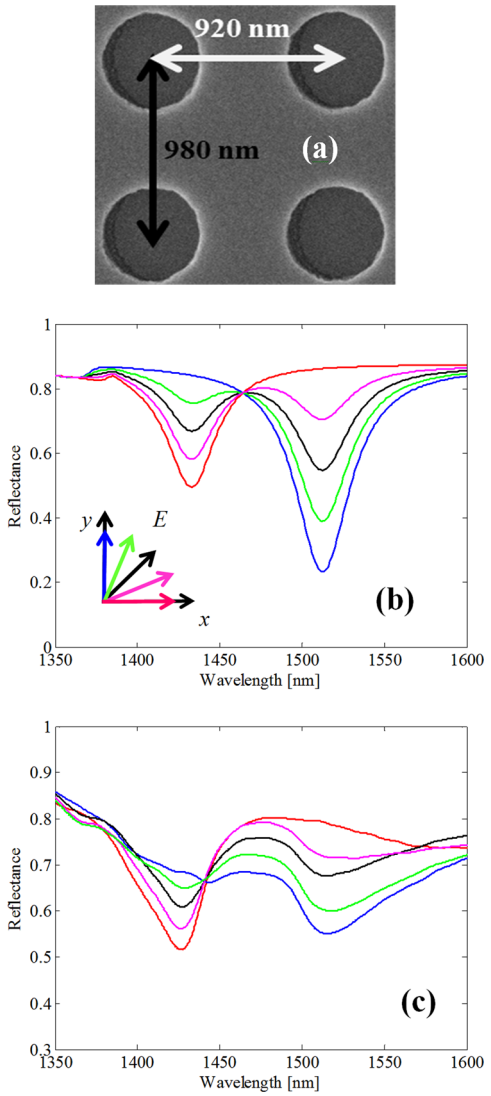

Figure 8. (a) SEM image (top view, zoomed) of the PCC probe with period asymmetry (a_x = 920 nm, a_y = 980 nm); (b) numerical and (c) experimental reflectance spectra of sample B for different incident wave polarizations: blue and red lines refer to POL_x and POL_y.

different distances along the two perpendicular axes, namely a_x = 920 nm and a_y = 980 nm (see SEM top-view image in Figure 8a). The hole diameter is kept constant to 450 nm.

In Figure 8b,c we report the numerical and experimental reflectance spectra for different incident wave polarizations, in good agreement with each other. Differently from the above case, since the two orthogonal polarization states interact with different lattice period, the plasmonic resonance excitation occurs at two different wavelengths. In particular, two different LSPRs are excited at ~1430 and ~1510 nm for POL_x to POL_y, respectively. This is in accordance with the fact that the smaller is the period, the smaller is the wavelength at which the resonant phenomenon takes place.

Clearly, when the incident electric field polarization gradually moves from one polarization to the other, we observe a sort of energy balance effect between the two resonant dips in the reflection spectrum: they basically undergo changes in their shape and visibility, appearing and disappearing at the two resonant wavelengths, as a function of the polarization.

In this case, our fiber probe works as a polarization-dependent, wavelength-selective device that could be used as a tunable polarization filter as well as a modulator.

The possibility to discriminate between perpendicular polarizations of the incoming light could be also exploited in quantum computing and quantum cryptography technologies, where an attempt to measure information encoded in the state of a photon results in a detectable disturbance.[39] We wish to stress and remark that the above experimental results are only preliminary and no efforts have been made to optimize the performances of the final device.

CONCLUSION

In conclusion, we have discussed the potentiality and versatility of an optical nanoprobe constituted by a hybrid metallo dielectric structure realized on a single mode optical fiber tip. The device has been fabricated through a valuable fabrication process enabling the integration onto optical fibers of functional materials at micro- and nanoscale. We have demonstrated how by selecting a specific dielectric and metal layer thickness it is possible to make the fiber tip device more or less sensitive to the external environment refractive index, thus, tailoring its performances for the specific applications. In

dx.doi.org/10.1021/ph400075r | ACS Photonics 2014, 1, 69−78

particular, by choosing a thick enough gold layer it is possible to obtain a strong plasmonic effect with low sensitivity to the external medium variations. Many degrees of freedom can be further exploited to increase the sensitivity: for example, we have preliminarily found that by exploiting a quasi-periodic tiling it is possible to significantly increase (up to a factor 2) the SRI bulk sensitivity with respect to the periodic case.

We have also investigated the surface sensitivity of the proposed devices, which in turn can be considered the key parameter when dealing with chemical and biological applications. Experimental results have revealed the capability to detect nanosized overlays deposited on the sensor substrate, demonstrating the effectiveness of the proposed platform to be used as high sensitivity label free biosensor. We have analyzed the effect of the metallo-dielectric crystal size on the spectral features exhibited by the integrated platform demonstrating that the sensitive area (i.e., the patterned area on the fiber tip) can be reduced down to only $20 \times 20\ \mu m^2$ without affecting the sensor operability; this foresees improved limits of detection in terms of number of bound biomolecules on the functionalized sensor surface for a given local refractive index change.

Concerning the plasmonic resonance engineering, as a result of a numerical analysis, it has been found that by acting on the dielectric layer thickness it is possible to increase the number and tailor the near field distributions of different plasmonic modes excited at different wavelengths. The near field distribution determines the sensitivity performances and regulates the light matter interaction. We have finally shown that the resonance engineering could be also achieved by acting on the lattice tiling; by breaking the circular symmetry of our device (with creating elliptical holes or different periods in the two perpendicular directions) it is possible to obtain polarization sensitive devices.

It is clear that the results discussed in this work, although they demonstrate the great versatility of the lab on fiber technology, reveal only a little part of what can be effectively achieved using this technology. To give an example, in addition to metallic structures supporting SPR, also metamaterials could be integrated on the optical fiber tip; thus, the creation of periodic distributions of subwavelength sized metal resonators could potentially open the way to novel devices exhibiting the exotic optical properties offered by metamaterials such as superlensing and cloaking.[40]

One senses that the potentialities offered by this technology have not yet been entirely exploited. Under many points of view, we are only at the beginning, especially in the fields of medical and biological applications. First, fiber optic nanoprobes could be judiciously integrated with microfluidics components to provide new lab on chip implementations, taking advantage from the easier connection of the optical chain to complex lighting systems as well as sophisticate interrogation units. Moreover, the real point of strength of this technology is certainly the property of allowing in vivo analysis; since optical fibers can be easily inserted inside medical needles, the remote interrogation of optical devices integrated on the fiber tip can provide in situ, real-time monitoring of different biological events such as molecular binding or tissues characterization. Indeed, as demonstrated in refs 5 and 26, the incorporation of an array of gold optical pillars onto the fiber facet can give rise to optical probes for surface enhanced Raman scattering (SERS) detection. Furthermore, by integrating and patterning soft materials (with a low Young modulus), it could be possible to realize very sensitive pressure sensors for elastometric measurements and characterization of human tissues. As already partially demonstrated in ref 27, the pressure wave impinging on the fiber tip causes physical deformations of the nanostructured layer, resulting in a resonance shift due to changes in the phase-matching condition. This phenomenon could be, in principle, exploited also for ultrasound detection, leading to the creation of fiber-based ultrasonic receivers for novel in situ ecography systems.

Lab-on-fiber technology devices could provide significant improvements also in the field of in vivo optical imaging techniques.[41] Nanoscale slit or holes arrays in a metallic film integrated on the optical fiber tip could be used as planar lenses whose focusing effect could further improve the imaging resolution.[42] Anyway, also in this latter case, differently from free space approaches, fiber-based devices (as those discussed in this work) and interrogation setups strongly facilitate in vivo applications. On the same line of argument, concerning noninvasive optical imaging method, polarization sensitive fiber-based devices could be effectively used in polarization sensitive optical coherence tomography (PS-OCT), which extends the concept of OCT providing cross-sectional images of tissue structure in real time. The change in polarization state of backscattered light (with respect to the polarization state of incident light) provides additional information about the properties of tissues and image contrast enhancement.[43] In order to fully take advantage of the filtering properties, however, it could be necessary to introduce electrical contacts in such a way to realize active device guaranteeing a better polarization control.

To conclude, although further investigations lie ahead and there is still so much to prove, it is fair to predict that the development of the lab on fiber technology (including all the related fabrication methods) is pointing to a novel class of multifunctional nanoprobes, with unique properties in terms of functionality, performances, and miniaturization.

METHODS

Sample Fabrication. Our fabrication process essentially consists of three main technological steps: (i) spin coating deposition of electron beam resist (and in particular electron beam resist like ZEP 520-A) with accurate thickness control and flat surface over the fiber core region; (ii) EBL nanopatterning of the deposited resist; and (iii) superstrate deposition of different functional materials, either metallic or nonmetallic, by using standard coating techniques (e.g., sputtering, thermal evaporation, etc). One of the main peculiarities of this approach relies on the capability to deposit dielectric layers on the cleaved end of optical fibers with controllable thickness and flat surface over an area of about 50 μm in diameter in correspondence of the fiber core. In order to adapt well-assessed nanoscale deposition and patterning techniques (typically used for planar devices) to directly operate on the fiber tip, we realized a customized chuck[27] to host the fiber for the spin coating process and a set of metallic holders enabling a suitable (perpendicular) fixing of the fiber facet for the overlay patterning and superstrate deposition. In particular, in order to deposit the e-beam resist onto the fiber tip, the latter one was inserted in the straight upward position, inside the customized chuck, keeping the fiber tip outside the plate. Successively, e-beam resist overlays, with different thicknesses, were obtained by using different rotating speed (in the range 2000−6000 round per minute) and deposition cycles. The spin coating process is then concluded by baking

dx.doi.org/10.1021/ph400075r | ACS Photonics 2014, 1, 69−78

the ZEP 520-A at 180 °C. Once the fiber has been properly lodged on a metallic holder, the pattern was written by the EBL system (Raith 150) on the deposited resist. The acceleration voltage was 20 kV and the dose ranges from 50 to 60 $\mu C/cm^2$. After the ZEP developing, the realized structure was coated by a gold layer via DC magnetron sputtering in a vacuum system at a base pressure of 8×10^{-5} Torr. In order to evaluate the RI surface sensitivity, the thin SiO_2 superstrate was deposited onto the fiber tip device by means of an ultravacuum RF sputtering at a pressure of 3 mTorr with a rate of 3.5 Å/s.

Optical Characterization. In order to characterize the resonant behavior of the fabricated devices, we performed spectral reflectance measurements by illuminating the fiber tip with a broadband optical source (covering the wavelength range 1200−1700 nm) and redirecting the reflected light (via a 2 × 1 directional coupler) to an optical spectrum analyzer (Ando AQ6317C). In addition, to avoid any influence of the spectral features of the light source, as well as of the losses introduced by the optical chain, the sample reflectance was normalized by that of a fiber optic reference mirror, fabricated by depositing a 160 nm thick gold film on the facet of a standard single-mode fiber. Moreover, a fiber optic polarization controller was used for the characterization of the polarization sensitive devices.

Simulations. Our numerical studies are based on full-wave simulations (via the finite-element-based commercial software package COMSOL Multiphysics[29] (RF module) and dispersive lossy model for the gold refractive index.[44] Refractive indexes of SiO_2 and ZEP are 1.45 and 1.54, respectively. Periodic boundary conditions and port conditions are applied on the vertical and horizontal walls of the unit cell (see Figure 1d), respectively. Note that, in view of the mirror symmetries involved, the computational domain (i.e., the unit cell) can be further reduced to one-quarter of the unit cell with perfectly electric-conducting (PEC) and perfectly magnetic-conducting (PMC) in-plane terminations, compatible with normal-incidence illumination (any further details on the simulation method can be found in ref 27).

AUTHOR INFORMATION

Corresponding Authors

*E-mail: emanuela.esposito@cnr.it (E.E.).
*E-mail: a.cusano@unisannio.it (A.C.).

Author Contributions

†These authors contributed equally to this work (A.R. and M.C.).

Notes

The authors declare no competing financial interest.

ACKNOWLEDGMENTS

The kind assistance of Dr. Carmine Granata (CNR-ICIB) for the SiO_2 depositions is gratefully acknowledged.

REFERENCES

(1) Culshaw; Kersey, A. Fiber-optic sensing: a historical perspective. *J. Light. Technol.* **2008**, *26*, 1064−1078.
(2) Barnes, W. L.; Dereux, A.; Ebbesen, T. W. Surface plasmon subwavelength optics. *Nature* **2003**, *424*, 824−830.
(3) Genov, D. A.; Sarychev, A. K.; Shalaev, V. M.; Wei, A. Resonant field enhancements from metal nanoparticle arrays. *Nano Lett.* **2004**, *4*, 153−158.
(4) Kneipp, K.; Kneipp, H.; Itzkan, I.; Dasari, R. R. Surface-enhanced raman scattering and biophysics. *J. Phys.: Condens. Matter* **2002**, *14*, R597−R624.
(5) Smythe, E. J.; Dickey, M. D.; Bao, J. M.; Whitesides, G. M.; Capasso, F. Optical antenna arrays on a fiber facet for in situ surface-enhanced raman scattering detection. *Nano Lett.* **2009**, *9*, 1132−1138.
(6) Liu, X. F.; Sun, C. H.; Linn, N. C.; Jiang, B.; Jiang, P. Wafer-scale surface-enhanced raman scattering substrates with highly reproducible enhancement. *J. Phys. Chem. C* **2009**, *113*, 14804−14811.
(7) Klar, T. A.; Kildishev, A. V.; Drachev, V. P.; Shalaev, V. M. Negative-index metamaterials: going optical. *IEEE J. Sel. Top. Quantum Electron.* **2006**, *12*, 1106−1115.
(8) Cubukcu, E.; Yu, N. F.; Smythe, E. J.; Diehl, L.; Crozier, K. B. Plasmonic laser antennas and related devices. *IEEE J. Sel. Top. Quantum Electron.* **2008**, *14*, 1448−1461.
(9) Pendry, J. B.; Holden, A. J.; Robbins, D. J.; Stewart, W. J. Magnetism from conductors and enhanced nonlinear phenomena. *IEEE Trans. Microwave Theory Technol.* **1999**, *47*, 2075−2084.
(10) Valentine, J.; Zhang, S.; Zentgraf, T.; Ulin-Avila, E.; Genov, D. A.; Bartal, G.; Zhang, X. Three-dimensional optical metamaterial with a negative refractive index. *Nature* **2008**, *455*, 376−380.
(11) Atwater, H. A.; Polman, A. Plasmonics for improved photovoltaic devices. *Nat. Mater.* **2009**, *9*, 205−213.
(12) Schuller, J. A.; Barnard, E. S.; Cai, W.; Jun, Y. C.; White, J. S.; Brongersma, M. L. Plasmonics for extreme light concentration and manipulation. *Nat. Mater.* **2010**, *9*, 193−204.
(13) Consales, M.; Pisco, M.; Cusano, A. Lab-on-fiber technology: a new avenue for optical nanosensors. *Photonic Sens.* **2012**, *2* (4), 28914.
(14) Cubukcu, E.; Kort, E. A.; Crozier, K. B.; Capasso, F. Plasmonic laser antenna. *Appl. Phys. Lett.* **2006**, *89*, 0931201−0931203.
(15) Smythe, E. J.; Cubukcu, E.; Capasso, F. Optical properties of surface plasmon resonances of coupled metallic nanorods. *Opt. Exp.* **2007**, *15*, 7439−7447.
(16) Scheerlinck, S.; Taillaert, D.; Van Thourhout, D.; Baets, R. Flexible metal grating based optical fiber probe for photonic integrated circuits. *Appl. Phys. Lett.* **2008**, *92*, 0311041−0311043.
(17) Smythe, E. J.; Dickey, M. D.; Whitesides, G. M.; Capasso, F. A technique to transfer metallic nanoscale patterns to small and nonplanar surfaces. *ACS Nano* **2009**, *3*, 59−65.
(18) Lipomi, D. J.; Kats, M. A.; Kim, P.; Kang, S. H.; Aizenberg, J.; Capasso, F.; Whitesides, G. M. Fabrication and replication of arrays of single- or multicomponent nanostructures by replica molding and mechanical sectioning. *Nano Lett.* **2010**, *4*, 4017−4026.
(19) Lipomi, D. J.; Martinez, R. V.; Kats, M. A.; Kang, S. H.; Kim, P.; Aizenberg, J.; Capasso, F.; Whitesides, G. M. Patterning the tips of optical fibers with metallic nanostructures using nanoskiving. *Nano Lett.* **2011**, *11*, 632−636.
(20) Jung, I. W.; Park, B.; Provine, J.; Howe, R. T.; Solgaard, O. Highly sensitive monolithic silicon photonic crystal fiber tip sensor for simultaneous measurement of refractive index and temperature. *J. Light. Technol.* **2011**, *29*, 1367−1374.
(21) Scheerlinck, S.; Dubruel, P.; Bienstman, P.; Schacht, E.; Van Thourhout, D.; Baets, R. Metal grating patterning on fiber facets by UV-based nano imprint and transfer lithography using optical alignment. *J. Light. Technol.* **2009**, *27*, 1415−1420.
(22) Shambat, G.; Provine, J.; Rivoire, K.; Sarmiento, T.; Harris, J.; Vuckovic, J. Optical fiber tips functionalized with semiconductor photonic crystal cavities. *Appl. Phys. Lett.* **2011**, *99*, 1911021−1911023.
(23) Lerma Arce, C.; De Vos, K.; Claes, T.; Komorowska, K.; Van Thourhout, D.; Bienstman, P. Silicon-on-insulator microring resonator sensor integrated on an optical fiber facet. *IEEE Photonics Technol. Lett.* **2011**, *23*, 890−892.
(24) Dhawan, A.; Gerhold, M.; Muth, J. Plasmonic structures based on subwavelength apertures for chemical and biological sensing applications. *IEEE Sens. J.* **2008**, *8*, 942−950.
(25) Lin, Y.; Zou, Y.; Lindquist, R. G. A reflection-based localized surface plasmon resonance fiber-optic probe for biochemical sensing. *Biomed. Opt. Exp.* **2011**, *2*, 478−484.

(26) Yang, X.; Ileri, N.; Larson, C.; Carlson, T.; Britten, J.; Chang, A.; Gu, C.; Bond, T. Nanopillar array on a fiber facet for highly sensitive surface-enhanced Raman scattering. *Opt. Exp.* **2012**, *20*, 24819−24826.
(27) Consales, M.; Ricciardi, A.; Crescitelli, A.; Esposito, E.; Cutolo, A.; Cusano, A. Lab-on-fiber technology: toward multifunctional optical nanoprobes. *ACS Nano* **2012**, *6*, 3163−3170.
(28) Feng, S.; Darmawi, S.; Henning, T.; Klar, P. J.; Zhang, X. A miniaturized sensor consisting of concentric metallic nanorings on the end facet of an optical fiber. *Small* **2012**, *8*, 1937−1944.
(29) http://www.comsol.com.
(30) Stewart, M. E.; Anderton, C. R.; Thompson, L. B.; Maria, J.; Gray, S. K.; Rogers, J. A.; Nuzzo, R. G. Nanostructured plasmonic sensors. *Chem. Rev.* **2008**, *108*, 494−521.
(31) Crescitelli, A.; Ricciardi, A.; Consales, M.; Esposito, E.; Galdi, V.; Cutolo, A.; Cusano, A. Nanostructured metallo-dielectric quasi-crystals: towards photonic-plasmonic resonance engineering. *Adv. Funct. Mater.* **2012**, *22*, 4389−4398.
(32) Pisco, M.; Ricciardi, A.; Gallina, I.; Castaldi, G.; Campopiano, S.; Cutolo, A.; Cusano, A.; Galdi, V. Tuning efficiency and sensitivity of guided resonances in photonic crystals and quasi-crystals: a comparative study. *Opt. Exp.* **2010**, *18*, 17280−17293.
(33) Senechal, M. In *Quasicrystals and Geometry*; Senechal, M., Ed.; Press Syndicate of Cambridge University: NY, 1995; Ch.5.
(34) Ricciardi, A.; Pisco, M.; Cutolo, A.; Cusano, A.; O ' Faolain, L.; Krauss, T.; Castaldi, G.; Galdi, V. Evidence of guided resonances in photonic quasicrystal slabs. *Phys. Rev. B* **2011**, *84*, 0851351−0851359.
(35) Gallina, I.; Pisco, M.; Ricciardi, A.; Campopiano, S.; Castaldi, G.; Cusano, A.; Galdi, V. Guided resonances in photonic crystals with point-defected aperiodically-ordered supercells. *Opt. Exp.* **2009**, *17*, 19586−19598.
(36) Tsargorodskaya, A.; Nabok, A. V.; Ray, V. Ellipsometric study of the adsorption of bovine serum albumin into porous silicon. *Nanotechnology* **2004**, *15*, 703−709.
(37) Piscevic, D.; Knoll, W.; Tarlov, M. J. Surface plasmon microscopy of biotin-streptavidin binding reactions on UV-photo-patterned alkanethiol self-assembled monolayers. *Supramol. Sci.* **1995**, *2*, 99−106.
(38) Hu, J.; Sun, X.; Agarwal, A.; Kimerling, L. C. Design guidelines for optical resonator biochemical sensors. *J. Opt. Soc. Am. B* **2009**, *26*, 1032−1041.
(39) Clark, A. S.; Fulconis, J.; Rarity, J. G.; Wadsworth, W. J.; O'Brien, J. L. All-optical-fiber polarization-based quantum logic gate. *Phys. Rev. A* **2009**, *79*, 0303031−0303034.
(40) McPhedran, R. C.; Shadrivov, I. V.; Kuhlmey, B. T.; Kivsha, Y. S. Metamaterials and metaoptics. *NPG Asia Mater.* **2011**, *3*, 100−108.
(41) Ntziachristos, V. Fluorescence molecular imaging. *Annu. Rev. Biomed. Eng.* **2006**, *8*, 1−33.
(42) Fu, Y.; Zhou, X. Plasmonic lenses: a review. *Plasmonics* **2010**, *5*, 287−310.
(43) de Boer, J. F.; Milner, T. E.; van Gemert, M. J. C.; Nelson, J. S. Two-dimensional birefringence imaging in biological tissue by polarization-sensitive optical coherence tomography. *Opt. Lett.* **1997**, *22*, 934−936.
(44) Palik, E. D. In *Handbook of Optical Constants of Solids*; Palik, E. D., Ed; Academic Press: Orlando, FL, 1985; Ch. 2.